Effects of columnar disorder on flux-lattice melting in high-temperature superconductors

Sandeep Tyagi and Yadin Y. Goldschmidt

Department of Physics and Astronomy, University of Pittsburgh, Pittsburgh, Pennsylvania 15260, USA
(Received 8 November 2002; revised manuscript received 5 February 2003; published 3 June 2003)

The effect of columnar pins on the flux-lines melting transition in high-temperature superconductors is studied using path-integral Monte Carlo simulations. We highlight the similarities and differences in the effects of columnar disorder on the melting transition in $YBa_2Cu_3O_{7-\delta}$ (YBCO) and the highly anisotropic $Bi_2Sr_2CaCu_2O_{8+\delta}$ (BSCCO) at magnetic fields such that the mean separation between flux lines is comparable to the penetration depth. For pure systems, a first-order transition from a flux-line solid to a liquid phase is seen as the temperature is increased. When adding columnar defects to the system, the transition temperature is not affected in both materials as long as the strength of an individual columnar defect (expressed as a flux-line defect interaction) is less than a certain threshold for a given density of randomly distributed columnar pins. This threshold strength is lower for YBCO than for BSCCO. For higher strengths, the transition line is shifted for both materials towards higher temperatures, and the sharp jump in energy, characteristic of a first-order transition, gives way to a smoother and gradual rise of the energy, characteristic of a second-order transition. Also, when columnar defects are present, the vortex solid phase is replaced by a pinned Bose glass phase and this is manifested by a marked decrease in translational order and orientational order as measured by the appropriate structure factors. For BSCCO, we report an unusual rise of the translational order and the hexatic order just before the melting transition. No such rise is observed in YBCO.

I. INTRODUCTION

Type-II superconductors[1–3] allow for a partial penetration of magnetic field into the bulk of the superconducting (SC) material when the applied field H satisfies $H_{c1} < H < H_{c2}$. In a seminal work Abrikosov[4] showed that when the ratio λ/ξ, where λ is the magnetic-field penetration depth and ξ is the coherence length, is greater than $1/\sqrt{2}$, the magnetic-field penetrates the SC material in the form of flux lines (FL's). These FL's are also called vortices, since they are surrounded by circular currents. Each FL carries a quantized unit of flux $\phi_0 = hc/2e$ called the fluxoid. The FL's have cylindrical shape of radius $\approx \lambda$ (the radius is not sharp since the magnetic-field decays exponentially like $\exp(-r/\lambda)$, where r is the distance from the axis) and a non-SC core of radius $\approx \xi$. Due to a repulsive interaction among the FL's, they arrange themselves in a triangular lattice referred to as the vortex solid (VS). This result follows from mean-field theory.

After high-temperature superconductors were discovered in the 1980's, it became apparent that thermal fluctuations, not included in the mean-field theory,[5] play an important role at relatively high temperatures and fields, still below T_c and H_{c2}. These fluctuations can cause the Abrikosov lattice to melt into a disordered liquid via a first-order transition (FOT), which can be roughly estimated using the Lindemann criterion known from solid-state physics.[6–8] Technologically, the melting of the FL lattice is important since the vortex liquid (VL) is not actually SC due to the dissipation caused by the FL motion when an electric current passes through the system. Pinning of FL's by naturally occurring defects in the form of vacancies, interstitials, twin and grain boundaries, etc., is effective to impede the FL motion in the VS phase, where the FL's form a rigid correlated network. The effectiveness of the pinning manifests itself by leading to high

critical currents. In the VL phase, pinning of a few vortices does not inhibit others from moving when a current is applied. Thus, for practical purposes the sudden increase in resistivity occurs at the melting transition rather than when $H = H_{c2}(T)$ for any reasonably nonvanishing currents.

The existence of the melting transition in high-T_c pristine materials has been established through numerous experimental[9–13] and numerical[14–20] studies. As was mentioned above, disorder in the form of points defects and sometimes more extended defects can and does occur naturally in laboratory samples. In addition, artificial point defects can be induced by bombarding the sample with electrons originating from particle accelerators. Extended columnar defects in the form of linear damaged tracks piercing through the sample can be induced by heavy-ion irradiation. Both naturally occurring and artificially induced defects are situated at random positions in the sample and their effective pinning strength (i.e., their interaction with FL's) can also vary from defect to defect. Thus, defects play the role of quenched disorder. The adjective "quenched" refers to the immobility of these defects during experimental time scales. Introduction of disorder in terms of point defects or columnar pins affects both the properties of the solid and liquid phases and might also shift the location of the melting transition in the H-T plane.[2,3] In the case of point pins, the VS phase is replaced with a Bragg-glass phase,[21,22] characterized by quasi-long-range order. The melting transition is predicted to shift towards lower temperatures.[23–25] In the case of columnar pins, the VS phase is replaced with a so-called pinned Bose glass,[26] where FL's are trapped by the columnar defects and the whole lattice becomes immobile. The Bose glass phase is similar to the localized phase of a two-dimensional repulsive Bose gas in the presence of quenched disorder, as will be explained in more detail in the following section.

The effect of both kinds of disorders on the FL's melting has been studied experimentally in various high-temperature superconductors. Two common materials that have been extensively investigated are $YBa_2Cu_3O_{7-\delta}$ (YBCO) and $Bi_2Sr_2CaCu_2O_{8+\delta}$ (BSCCO), both having critical temperatures ranging between 90–120 K at $H=0$. The main difference between these materials is their anisotropy parameter $\gamma^2 = m_z/m_\perp > 1$, where m_z and $m_\perp$ denote the effective masses of electrons moving along the c axis and the ab plane, respectively. BSCCO is much more anisotropic: its anisotropy parameter γ lies in the range of 50–200 compared to the range of 5–7 for YBCO.[2] This fact causes the FL's to be much "softer" or elastic. Thus, in the case of BSCCO the FL's are sometimes described as a collection of loosely connected "two-dimensional droplets" residing in adjacent Cu-O planes. Experimental studies on YBCO have shown a marked shift in the irreversibility line in the presence of the columnar disorder.[27-31] The irreversibility line in the H-T plane marks the onset of hysteresis effects and is located close to the melting transition on the solid phase side. For BSCCO, many experimental studies have been conducted.[32-39] The more recent ones have shown[36-39] that the melting line is not shifted when the density of columnar defects is relatively low, $B_\phi \ll B$, but for $B_\phi \approx B$, a shift in the position of the melting transition is observed. Here, the matching field B_ϕ is defined as $B_\phi = n_d \phi_0$, where n_d is the density of the columnar defects and ϕ_0 is the flux quantum.

Theoretical work on columnar disorder includes Bose glass theory.[26] Radzihovsky[40] considered the possibility of two kinds of Bose glass phases (strongly or weakly pinned) depending on whether $B < B_\phi$ or $B > B_\phi$. More recently, columnar as well as point disorder were investigated by Goldschmidt[25] using replica field theory. He showed that the melting line shifts to lower temperature in the case of point disorder and to higher temperature in the case of columnar disorder.

Due to the complexity of the problem, especially in the presence of disorder, simulations have been very useful in studying the FL system. There have been many simulation studies of the vortex system in the presence of disorder. However, most simulation work has been confined to the addition of point disorder only. In particular, there is little work done on the effects of columnar disorder on the FL melting. Recent work by Wengel and Täuber[41] concentrated on the case of high defect density region $B_\phi \approx B$. In contrast, a recent simulation study by Sen *et al.*[42] uses a small density of columnar defects, each of infinite strength, but considers an extremely small magnetic field. Similarly, Nandgaonkar *et al.*[43] also investigate the case of a very small magnetic field. In this paper, we consider columnar defects of a finite strength η with a relatively low defect density, $B_\phi/B = 0.2$, and with realistic magnetic fields as used in the experiments.

II. THE MODEL

We first discuss the method implemented for YBCO.

Following Nelson,[44] we map the system of N vortices (FL's) in a high-T_c superconductor onto N interacting bosons in two-space + one-time dimensions. Then, we do a path-

integral Monte Carlo (PIMC) simulation on this system. The partition function of N vortices can be expressed as

$$\Xi(T,L_z,N) = e^{-F(T,L_z,N)/kT} = \frac{1}{N!} \int \prod_{i=1}^{N} D\mathbf{R}_i(z) e^{-\Im/kT},$$
(2.1)

where $\mathbf{R}_i(z)$ denotes the two-dimensional (2D) position vector of the ith vortex at a height z along the c axis, F is the free energy as a function of temperature T, L_z is the length of the sample along the z direction. The London free-energy functional $\Im$ is given by

$$\frac{\Im}{kT} = \frac{1}{kT} \int_0^{L_z} dz \left\{ \sum_i \frac{\varepsilon_l}{2} \left(\frac{d\mathbf{R}_i}{dz} \right)^2 + \sum_{i<j} 2\varepsilon_0 K_0 \left(\frac{R_{ij}}{\lambda} \right) \right\},$$
(2.2)

where $\varepsilon_0 = \phi_0^2/(4\pi\lambda)^2$ is the vortex line energy per unit length, the line tension is $\varepsilon_l = \varepsilon_0 \ln(a_0/2\sqrt{\pi}\xi)/\gamma^2$, and $R_{ij}(z) = |\mathbf{R}_i(z) - \mathbf{R}_j(z)|$. Here,

$$a_0 = \sqrt{\frac{2\phi_0}{\sqrt{3}B}}$$
(2.3)

is the lattice spacing, B is the magnetic field along the z direction, and γ is the anisotropy parameter. $K_0(R_{ij}/\lambda)$ is the in-plane interaction potential between two FL's a distance R_{ij} apart. K_0 denotes the modified Bessel function of the first kind. This expression for the London free-energy is an approximation that neglects the nonlocal interaction of real vortices and replaces it by in-plane interactions only, which is really justified if the FL's do not deviate too much from straight lines along the z axis.[19] With this approximation, the system of N interacting FL's is equivalent to a system of N bosons in $d=2$ dimension interacting with a pairwise potential $K_0(R_{ij}/\lambda)$.

The path-integral representation of a system of N bosons of mass m each in two dimensions, interacting through a potential $V(r) = g^2 K_0(r/\lambda)$, with g being the strength and λ being the range of the repulsive interaction, is given at finite temperature T_B in terms of the imaginary time action

$$\frac{S}{\hbar} = \frac{1}{\hbar} \int_0^{\hbar/kT_B} d\tau \left\{ \sum_i \frac{m}{2} \left(\frac{d\mathbf{R}_i}{d\tau} \right)^2 + \sum_{i<j} g^2 K_0 \left(\frac{R_{ij}(\tau)}{\lambda} \right) \right\}.$$
(2.4)

Here, τ is the imaginary time and T_B is the temperature of the Bose system. We see that there is a one to one parameter mapping between the boson system and the vortex system:[19]

$$\tau \to z, \quad \hbar \to kT, \quad g^2 \to 2\varepsilon_0, \quad \hbar/kT_B \to L_z, \quad m \to \varepsilon_l,$$

$$n = N/A = 2/(\sqrt{3}a_0^2) = B/\phi_0,$$

where n is the average density of bosons (and FL's) and A is the area of the sample. We can write the London free-energy functional in a dimensionless form as follows:

$$\frac{\Im}{kT} = \int_0^\beta d\tau \left\{ \sum_i \frac{1}{2\Lambda^2} \left(\frac{d\mathbf{R}_i}{d\tau} \right)^2 + \sum_{i<j} K_0 \left(\frac{R_{ij}}{\tilde{\lambda}} \right) \right\}, \quad (2.5)$$

where

$$\Lambda = \frac{\hbar}{a_0 g \sqrt{m}} = \frac{kT}{a_0 \sqrt{2\varepsilon_l \varepsilon_0}}, \quad \beta = \frac{g^2}{kT_B} = \frac{2\varepsilon_0 L_z}{kT}, \quad \tilde{\lambda} = \frac{\lambda}{a_0}. \tag{2.6}$$

All lengths are measured in units of a_0 and energies in units of g^2 for bosons and $\varepsilon_0 a_0$ for FL's. We next discretize the integral along the z axis by dividing it into M segments

$$\Xi(\beta, \Lambda, T)$$
$$= \frac{1}{N!} \left(\frac{1}{2\pi\Lambda^2\tau} \right) \sum_P \int \prod_{m=1}^{M} \prod_{i=1}^{N} d^2\mathbf{R}_{i,m} e^{-\Im[\mathbf{R}_{i,m}]/kT}, \tag{2.7}$$

where $\tau = \beta/M$, m labels the planes and

$$\frac{\Im[\mathbf{R}_{i,m}]}{kT} = \sum_{i,m} \frac{(\mathbf{R}_{i,m+1} - \mathbf{R}_{i,m})^2}{2\Lambda^2\tau} + \sum_{i<j} \tau K_0(R_{ij,m}/\tilde{\lambda}). \tag{2.8}$$

We work only in the limit where β is large, which amounts to taking L_z very large and in the mapping onto 2D bosons corresponds to the ground state of the bosons at the absolute zero temperature ($T_B = 0$). We used $\beta = 375$ and discretized the z axis into $M = 75$ planes.

We used the matrix-squaring method[45,46] to calculate the right action so that we can work with a small number of planes along the z direction. Working with the primitive action requires the use of a large number of slicing of the z direction and is very time consuming.[46] The boundary conditions in the z direction for a system of bosons are $\mathbf{R}_i(\beta) = \mathbf{R}_j(0)$, with all permutations $j = P(i)$ of the indices being allowed. This is what is meant by the summation over P in Eq. (2.7). For small g (a small repulsive interaction), which corresponds to large Λ, we expect a Bose-Einstein condensed phase where permutations are important. This is the superfluid phase. For small Λ, repulsion is large and permutations are rare as the Bose system is in its classical phase which is a Wigner crystal. These two phases correspond, respectively, to the FL liquid and solid phases. The melting line represented by $\Lambda = \Lambda_m$ is given approximately by the expression $B_m = \text{const}/T^2$. Near T_c this behavior is more complicated (see below).

We now discuss the method of simulations of BSCCO.

Because of the high anisotropy of the BSCCO system one cannot use the simple picture given above. Here, instead, we follow a different model that can be cast in a form analogous to YBCO. We take the Lawrence-Doniach model[47] as our starting point for BSCCO. It leads to the following form of the London free-energy for interlayer (IL) Josephson coupling:[16,48]

$$\Im_{IL}(\mathbf{R}_{i,m}) = \frac{d\phi_0^2}{8\pi^3\lambda^2} \left[1 + \ln\left(\frac{\lambda}{d}\right) \right] \left[\frac{(|\mathbf{R}_{i,m} - \mathbf{R}_{i,m+1}|)^2}{4r_g^2} - 1 \right], \tag{2.9}$$

for $|\mathbf{R}_{i,m} - \mathbf{R}_{i,m+1}| < 2r_g$ and

$$\Im_{IL}(\mathbf{R}_{i,m}) = \frac{d\phi_0^2}{8\pi^3\lambda^2} \left[1 + \ln\left(\frac{\lambda}{d}\right) \right] \left[\frac{|\mathbf{R}_{i,m} - \mathbf{R}_{i,m+1}|}{r_g} - 2 \right], \tag{2.10}$$

for $|\mathbf{R}_{i,m} - \mathbf{R}_{i,m+1}| > 2r_g$, where d is the interlayer spacing and r_g is the healing length defined by $r_g = \gamma d$. For the in-plane (IP) coupling, we use

$$\Im_{IP}(\mathbf{R}_{ij,m}) = \frac{d\phi_0^2}{8\pi^2\lambda^2} K_0\left(\frac{R_{ij,m}}{\lambda}\right). \tag{2.11}$$

In principle, one should add to the above interaction an electromagnetic interaction among the two-dimensional droplet vortices.[49] The electromagnetic interaction becomes dominant in the limit of infinite anisotropy ($\gamma \to \infty$). Ryu *et al.*[16] argue, (see also Ref. 50) that for the values $\gamma = 50 - 100$ for BSCCO the Josephson coupling still dominates over the electromagnetic coupling. Their argument goes as follows: Clem[49] shows that if one has a straight array of two-dimension droplet vortices along the z axis and one two-dimensional droplet is displaced by a distance R in the x direction than the magnetic energy of the configuration increases by an amount

$$\Delta E(R) = \frac{d\phi_0^2}{8\pi^2\lambda^2} \left[\mathcal{C} + \ln\left(\frac{R}{2\lambda}\right) + K_0\left(\frac{R}{\lambda}\right) \right], \tag{2.12}$$

where $\mathcal{C}$ is Euler's constant ($= 0.5772 \ldots$). For large R ($R \gg \lambda$), the modified Bessel function K_0 decays exponentially and thus the energy increases like $\ln(R/\lambda)$. For small R, the Bessel function can be expanded in a power series in R/λ

$$K_0(R/\lambda) = -\ln(R/2\lambda)(1 + R^2/4\lambda^2 + \cdots)$$
$$- \mathcal{C} + R^2(1 - \mathcal{C})/4\lambda^2 + \cdots, \tag{2.13}$$

and thus the magnetic energy behaves like R^2 to a leading order in R which is the same as the quadratic behavior of the Josephson energy in Eq. (2.9) above. The ratio of the coefficients of the quadratic terms in the magnetic and Josephson energies goes roughly like $\gamma^2(d/\lambda)^2$ (where $d/\lambda \sim 1/100$ for BSCCO at $T = 0$ and even smaller at higher temperatures). Thus for anisotropy $\gamma = 50$, we get a factor of 0.25 or less (a somewhat more precise estimate[16] gives a ratio of about 0.1). Thus, the magnetic interaction is small compared to the Josephson interaction for anisotropies in the range of $\gamma = 50 - 100$. For samples with $\gamma = 200$ these interactions are already comparable. For large values of R, the magnetic interaction increases logarithmically and the Josephson interaction increases linearly so the magnetic interaction is always negligible. The key to the estimate given above is to consider not just two two-dimensional droplet vortices but a whole line with one displaced two-dimensional droplet. This argument is valid if the deviations of the vortices from straight lines are not too large. As for the in-plane interaction Clem showed that a linear array of two-dimensional droplet vortices gives rise to exactly the same magnetic field at a distance R away from it as produced by an Abrikosov vortex line. Thus, Eq. (2.11) is consistent with the magnetic interaction

of two-dimensional droplet vortices, again when the FL's do not deviate too much from straight lines.

Equations (2.9)–(2.11) for BSCCO can be cast in a form similar to that for the YBCO with the following substitutions:

$$\Lambda = \frac{kT}{\varepsilon_0 a_0} \frac{r_g}{d} \sqrt{\frac{\pi}{2\left[1+\ln\left(\frac{\lambda}{d}\right)\right]}}, \quad \tau = \frac{2\varepsilon_0 d}{kT}.$$

(2.14)

With these changes the London free-energy functional would look like

$$\frac{\Im_{IL}(\mathbf{R}_{i,m})}{kT} = \left[\frac{(|\mathbf{R}_{i,m}-\mathbf{R}_{i,m+1}|)^2 - r_g^2}{2\Lambda^2 \tau}\right],$$

(2.15)

for $(|\mathbf{R}_{i,m}-\mathbf{R}_{i,m+1}|) < 2r_g$ and

$$\frac{\Im_{IL}(\mathbf{R}_{i,m})}{kT} = \left[\frac{(\mathbf{R}_{i,m}-\mathbf{R}_{i,m+1})^2 - r_g^2}{2\Lambda^2 \tau}\right] - \frac{[2r_g-(|\mathbf{R}_{i,m}-\mathbf{R}_{i,m+1}|)]^2}{2\Lambda^2 \tau},$$

(2.16)

for $(|\mathbf{R}_{i,m}-\mathbf{R}_{i,m+1}|) > 2r_g$, when now again all lengths are measured in units of a_0. While doing simulations at a fixed magnetic field B and temperature T, the term $r_g^2/2\Lambda^2 \tau$ will remain constant and would drop out of ΔE term in the Boltzmann factor. It, however, need to be considered during the measurement of the energy. The second term in Eq. (2.16) can be easily handled at the last stage of the bisection method (see the following section for a discussion of the bisection method).

We can make use of a reduced temperature variable to make some expressions look simpler. First, using the fact that the temperature dependence of Λ arises mainly through ε_0 and neglecting the logarithmic corrections, one gets[2,16,15]

$$\lambda = \frac{\lambda_0}{\sqrt{1-T/T_c}}, \quad \varepsilon_0 \propto \frac{1}{\lambda^2} \propto \left(1-\frac{T}{T_c}\right),$$

(2.17)

and hence

$$\Lambda \propto \frac{T\sqrt{B}}{1-T/T_c}.$$

(2.18)

Defining reduced temperature as

$$T_r = \frac{T}{1-T/T_c},$$

(2.19)

we obtain

$$\Lambda \propto T_r \sqrt{B}.$$

(2.20)

This shows that the equation for the melting line is approximately

$$B_m = \text{const}(1-T/T_c)^2/T^2.$$

Note that some authors[51] use a temperature dependence of $1/\sqrt{1-T^2/T_c^2}$ in λ, or even[1] $1/\sqrt{1-T^4/T_c^4}$. All these choices coincide near T_c. The choice of temperature dependence of λ is not expected to have a significant effect on the results.

III. NOTES ON THE SIMULATIONS

The technique that we use to simulate our system is called multilevel Monte Carlo simulation (MMC).[46] There are several advantages in using this technique for the simulation of the FL's over the usual metropolis Monte Carlo (MC) method. In the discrete model, we work with N FL's with the z axis discretized into M planes, thus resulting in N beads in each of the M planes. In the usual MC method, one would displace a few of these beads in a plane by small random displacements inside a two-dimensional box and then would accept or reject the move based on a probability given by the Boltzmann factor.

A big disadvantage of using this technique is that it is difficult to move beads appreciably from their original positions over a number of MC steps. The reason for this is that a bead in a plane belonging to a FL finds itself in a local harmonic potential generated by the kinetic-energy term involving this bead and the beads belonging to the same FL on either side of the plane. This harmonic potential becomes stronger and stronger at lower temperatures and magnetic fields. As a result, in the usual MC simulations beads keep moving around inside these local harmonic cages and end up sampling only a small part of the phase space. The other problem with the usual MC method is that there is no natural easy way of implementing FL cutting. If there are two FL's twisted around each other and if it is energetically favorable for them to reconnect each other in such a way as to lower their free energy then this step should be permitted in the MC method without regard to the question if this process occurs in reality. This is so because in the MC simulations phase space is sampled according to the probability distribution and all one needs is to generate configurations weighted by the Boltzmann factor, and the path followed in configuration space has nothing to do with any real dynamics.

These two main drawbacks of the usual MC method are easily overcome in the MMC technique. First, one moves bigger chunks of FL's encompassing beads in several planes. This way one can avoid local harmonic traps. (This is like taking an aerial route to a destination rather than going through the zigzag maze of roads.) This is much in the spirit of Fourier space Monte Carlo where one first samples modes with smaller wave numbers and then move onto higher modes.

The method of creating new FL configurations is based on the concept of the conditional probabilities. It is called the bisection method[46] because one starts sampling beads by iteratively bisecting the FL's. At each stage of the division, the beads belonging to that stage are moved with some conditional probability factor P_i. It is important to make sure that the probabilities are chosen in such a way that detailed balance is satisfied at each stage of the division. One notes that the P_i's may not be the actual Boltzmann factors for the beads to be moved at different levels. But what is required is

that when all P_i's are multiplied together, they cancel in such a way so as to leave the correct Boltzmann factor for the whole move. Thus, inherent in this algorithm is the fact that a move would finally be accepted only if it has been accepted at each stage of the bisection method. The power of this method lies in choosing the appropriate P_i's. If these conditional probability factors are chosen judiciously, most of the rejections would take place at the initial stages of the bisection process when not too much computational effort has been spent yet.

The cutting and reconnection of FL's is implemented naturally in a MMC method: permutation among the three or four lines chosen to be moved becomes the first among the many hierarchical steps one goes through before a move is finally accepted and the position of the beads updated accordingly. We typically moved a total of 15–20 beads distributed over five planes. Permutations were sampled by a random-walk algorithm through the space of permutations[19] (see Appendix B).

In the case of YBCO, we worked with a field of $B = 4000$ G. Working in the primitive approximation of the action would require the use of a smaller value of the dimensionless parameter τ, which would require slicing of the z direction into a large number of planes. To avoid this, the matrix-squaring method[45,46] has been used to get the effective action for bigger values of τ. For example, Nordborg and Blatter[19] use a value of $\tau=3.0$ and they work with 100 planes. In this simulation, a value of $\tau=5.0$ has been used and the z axis has been sliced into 75 planes. Choosing a bigger value of τ by utilizing the matrix-squaring method makes it easier to equilibrate the system as compared to working with the primitive approximation.

For BSCCO, we did not use the matrix-squaring method because of the complications involved due to the few extra terms in free energy which contribute depending on whether R_{ij} is smaller or bigger than r_g. Here, we used the natural interlayer spacing d to calculate the parameter τ at different temperatures and then used the MMC technique to efficiently sample the configurational space.

As mentioned previously, in the present simulations we included only the Josephson coupling. This approximation works well with YBCO but it could be less satisfactory for BSCCO because of its high anisotropy. For very anisotropic materials, the electromagnetic coupling becomes important.[49,51] As discussed in Sec. II, Ryu *et al.*[16] estimated that for anisotropy of magnitude $\gamma=50-100$ the Josephson interaction still dominates over the electromagnetic interaction, but this will not be the case for $\gamma=200$ which may characterize some samples. Olson *et al.*[52] discuss how to include the electromagnetic interaction in a MC simulation, but they only consider the opposite limit where the Josephson coupling is totally neglected. To our knowledge, there is no satisfactory treatment of both couplings included on equal footings. We carried out preliminary simulations which show that the inclusion of the electromagnetic coupling does not shift the position of the transition line much at a field of 125 G, thus supporting our current conclusions. These results will be reported elsewhere.[53]

Simulations were usually carried out for 36 and 64 FL's.

The decay of the structure factors at the transition temperature becomes sharper when one uses a larger number of FL's. However, no appreciable shift in the transition temperature is seen, while working with the smaller ($N=36$) or the larger system ($N=64$). We did not run our simulations for even larger systems as it becomes computationally very time consuming. Typical simulation times were $\sim 3.5 \times 10^6$ MC steps. Each MC step involved moving three to four lines in five planes simultaneously. We usually averaged over 10–15 realizations of the columnar disorders, though some results have an average over as many as 20 realizations of the disorder.

Columnar disorder is modeled as an array of straight cylindrical wells of typical radius $r_d=25-35$ Å placed randomly throughout the cross-sectional region of the sample and oriented along the z direction.[2] Each columnar defect is of length L_z. The density of the columnar pins can be varied by changing their number for a given cross-sectional area, and the strength is controlled by a positive dimensionless parameter η. If a bead happens to wander inside a columnar well, we include an extra free energy of $-\eta(d\phi_0^2/8\pi^2\lambda^2)$. The defect concentration was taken to be a 20% ratio of defects to FL's which means $B_\phi/B=0.2$. The strength of disorder was set at $\eta\leq 0.5$ for BSCCO. For YBCO, $\eta=0.5$ was found to be too large in the sense that the transition became too broad and useful information could not be extracted. Thus, for YBCO, we kept $\eta\leq 0.3$.

Other parameters used for YBCO are $\gamma=5$, $\lambda_0 = 1500$ Å, $\xi_{ab}(0)=15$ Å, $d=12$ Å. Parameters for BSCCO are as follows: $\gamma=125$, $\lambda_0=1700$ Å, $\xi_{ab}(0)=20$ Å, $d = 15$ Å.

IV. MEASURED QUANTITIES

In this section, we describe many different physical quantities that were monitored during the simulation. From the variation of these quantities with the temperature we can extract important conclusions about the different phases of the system.

A. Energy

In terms of the reduced temperature, the energy

$$E = T^2 \frac{\partial}{\partial T} \ln[\Xi(\Lambda,\beta,N)] \tag{4.1}$$

can be simply written as:[19]

$$E = T_r(S_1 + S_2), \tag{4.2}$$

where (for BSCCO)

$$S_1 = \left\langle \sum_{m,i} \frac{(|\mathbf{R}_{i,m} - \mathbf{R}_{i,m+1}|)^2 - r_g^2}{2\Lambda^2\tau} \right\rangle$$

$$\text{for } (|\mathbf{R}_{i,m} - \mathbf{R}_{i,m+1}|) < 2r_g \tag{4.3}$$

and

$$S_1 = \left\langle \sum_{m,i} \left[\frac{(\mathbf{R}_{i,m} - \mathbf{R}_{i,m+1})^2 - r_g^2}{2\Lambda^2 \tau} \right. \right.$$

$$\left. \left. - \frac{[2r_g - (|\mathbf{R}_{i,m} - \mathbf{R}_{i,m+1}|)]^2}{2\Lambda^2 \tau} \right\rangle, \right. \quad (4.4)$$

for $(|\mathbf{R}_{i,m} - \mathbf{R}_{i,m+1}|) > 2r_g$, whereas

$$S_2 = \left\langle \sum_{m,i>j} \tau K_0\left(\frac{|\mathbf{R}_{i,m} - \mathbf{R}_{j,m}|}{\lambda} \right) \right\rangle. \quad (4.5)$$

Any discontinuous jump in E would indicate a FOT. From this discontinuous jump in energy, ΔE, we can also calculate the jump in entropy Δs,

$$\Delta s = \frac{\Delta E}{T}. \quad (4.6)$$

B. Translational structure factor

The translational structure factor $S(\mathbf{Q}_{l_1, l_2})$ is defined as

$$S(\mathbf{Q}_{l_1, l_2}) = \frac{1}{MN} \left\langle \sum_{ij,m} e^{[i\mathbf{Q}_{l_1, l_2} \cdot (\mathbf{R}_{i,m} - \mathbf{R}_{j,m})]} \right\rangle, \quad (4.7)$$

where $\langle \cdots \rangle$ stands for the MC average, $\mathbf{Q}_{l_1, l_2}$ is a reciprocal-lattice vector and is of the form

$$\mathbf{Q}_{l_1, l_2} = l_1 \mathbf{b}_1 + l_2 \mathbf{b}_2, \quad (4.8)$$

and l_1 and l_2 are some integers. $\mathbf{b}_{1,2}$ represent the basis vectors of the reciprocal lattice

$$\mathbf{b}_{1,2} = \frac{2\pi}{a_0 \sin^2 \theta} (\mathbf{e}_{1,2} - \mathbf{e}_{2,1} \cos \theta), \quad (4.9)$$

where $\theta = \pi/3$, a_0 is the nearest-neighbor distance, and $\mathbf{e}_{1,2}$ are the unit vectors along the hexagonal unit cell such that

$$\mathbf{e}_1 \cdot \mathbf{e}_2 = \cos \theta. \quad (4.10)$$

In the simulations, l_1 and l_2 in Eq. (4.7) are chosen to be 1 and 0 or 0 and 1. These choices correspond to the first Bragg peak. We will normally write $S(\mathbf{Q}_{1,0})$ as simply $S(\mathbf{Q}_1)$. This quantity gives important information about the phase of the system. In an ordered phase where FL's sit on a triangular lattice, $S(\mathbf{Q}_1)$ is of the order of N. In the disordered phase, it saturates to almost zero as the system size increases. In the simulations, however, there is a problem with measuring $S(\mathbf{Q}_1)$, especially in the presence of disorder. We will return to this point at the end of the section.

C. Hexatic structure factor

We use Delaunay triangulation to measure the hexatic order parameter ψ_6, which is defined as

$$\psi_6 = \left\langle \sum_{m=1}^{M} \sum_{i=1}^{N} \frac{1}{z_{i,m}} \sum_{j=1}^{z_{i,m}} e^{(i6\theta_{ij,m})} \right\rangle, \quad (4.11)$$

where $z_{i,m}$ denotes the number of the nearest neighbors of a bead at position i, m and it is six for a perfect hexagonal lattice, $\theta_{ij,m}$ stands for the bond angle, that is the angle that vector $\mathbf{R}_{ij,m}$ makes with an arbitrary axis. Just like the $S(\mathbf{Q}_1)$, this quantity too has a large value in an ordered phase and saturates at a finite value for a system of finite size.

D. Line entanglement

As we allow permutations of FL's, we can define a number N_e/N as that fraction of the total number of FL's which belong to loops that are bigger than the size of a "simple" loop. A simple loop is defined as a set of M beads connected end to end, M being the total number of planes. Loops of size $2M$, $3M$, ... start proliferating at and above the transition temperature and in the corresponding 2D boson system this proliferation is related to the onset of the superfluidity.

E. Line wandering

The transverse FL fluctuations are measured by

$$u^2(z) = \langle [\mathbf{R}(z_0 + z) - \mathbf{R}(z_0)]^2 \rangle / a_0^2, \quad (4.12)$$

which is independent of z_0. At the transition temperature $u^2(z)$ undergoes a large increase for large z.

We want to emphasize one important aspect of measuring the translational structure factor. The usual way of measuring this quantity is by choosing $\mathbf{Q}_{l_1, l_2}$ corresponding to the first Bragg peak, i.e., $\mathbf{Q}_1$ in Eq. (4.7). Now, it might happen that the configuration of the FL's comes close to making an almost perfect hexagonal lattice but its basis vectors are not aligned along the usual major axes of the rhombically shaped cell encompassing the system. If we use the reciprocal-lattice vector $\mathbf{Q}_1$ to measure the structure factor of such a configuration, we would end up getting a very small value for $S(\mathbf{Q}_1)$ and might wrongly conclude that the system is in a very disordered state. This happened many times in our simulations; we got a very low value of the translational structure factor, while the hexatic order was indicating a high degree of orderliness in the FL lattice. To remedy this situation, the translational structure factor is measured at 60 different angles, $1°$ apart, and choose that number which gives the largest possible value of the $S(\mathbf{Q}_1(\alpha))$ corresponding to some angle α. After implementing this technique, we find that $S(\mathbf{Q}_1)$ and ψ_6, which differ so much initially, almost follow each other.

V. RESULTS

(1) For YBCO, simulations were carried out at a magnetic field of $B = 4000$ G. At this field, we have $2a_0 \approx \lambda_0$. By the argument given in Ref. 19, we conclude that our results should hold qualitatively for any B such that $a_0 < \lambda$. We checked our simulation results against those by Nordborg and Blatter.[19] First, we verified that our code was working fine by comparing our results against those given in Ref. 19. Working in the limit of $L_z \rightarrow \infty$, we kept τ fixed as Λ was increased. We got a sharp transition at $\Lambda = 0.0605$. A jump
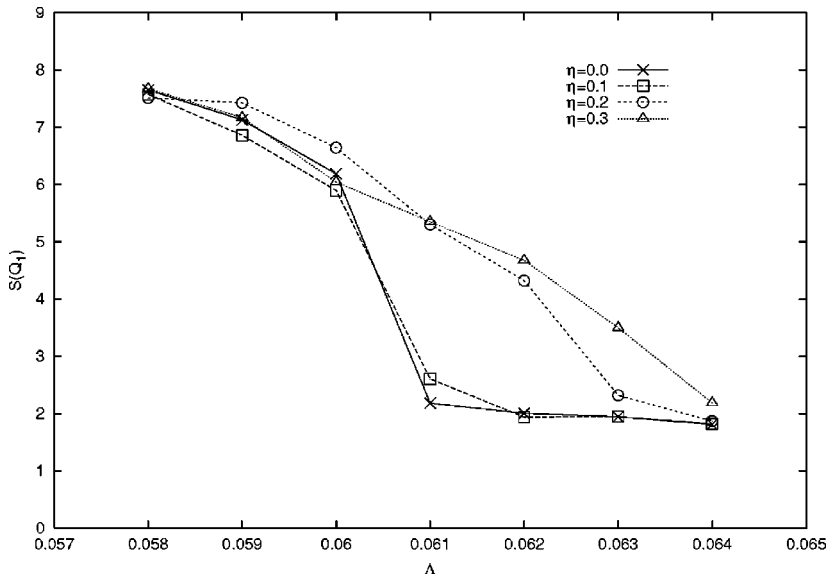
FIG. 1. YBCO: Structure factor at the first Bragg peak as a function of Λ at various disorder strengths η's for $N=36$. A clear shift in transition point towards higher Λ's is seen for $\eta \geq 0.2$.

was also seen in the energy as defined in the preceding section and was found to be $0.013k$, again the same as in Ref. 19.

The effect of introducing columnar disorder on the structure factor at the first Bragg peak is shown in Fig. 1. In Fig. 2, we depict the jump in the energy for a pure as well as for a disordered system.

We note that at lower strengths of the disorder, the melting line is almost unaffected and the transition takes place at $\Lambda \approx 0.0605$. However, as we increase the strength of the disorder, the melting transition shifts towards higher values of Λ which means that the melting line shifts towards higher temperatures and/or higher magnetic fields. For η up to 0.1 no change is seen in the melting curve or in the jump in the free-energy functional. However, at η equal to 0.2 the structure factor comes down at around 0.0625 and the jump in the energy becomes gradual. This finding is in agreement with several experimental studies where a change in the irreversibility line is seen with the introduction of columnar disorder.[27–31]

Next, we look at the FL entanglement. N_e denotes the number of FL's which do not form a simple loop. By looking at the N_e/N vs Λ graph in Fig. 3, it is clear that the entanglement is suppressed by as much as almost one order of magnitude just after and in the vicinity of the original transition line at $\Lambda = 0.0605$. This result is expected, as it is well known that point disorder helps in line wandering and entanglement, while the columnar disorder has just the opposite effect[25] since a nearby FL is induced to align along the columnar defect, and thus its transverse fluctuations are reduced. Unfortunately, there have been few studies on columnar disorder in YBCO. Sen et al.[42] work with vanishingly small magnetic field and infinite pinning strengths, in the vicinity of the lower branch of the melting line.

Figure 4 shows the effect of columnar disorder on a system of 64 FL's in YBCO. This graph shows a transition at almost the same Λ as in Fig. 1. This is a confirmation that finite-size effects are not important in our simulations.

(2) For the BSCCO system, the E vs T graphs for different η values are depicted in Fig. 5 (36 FL's) and Fig. 6 (64 FL's).
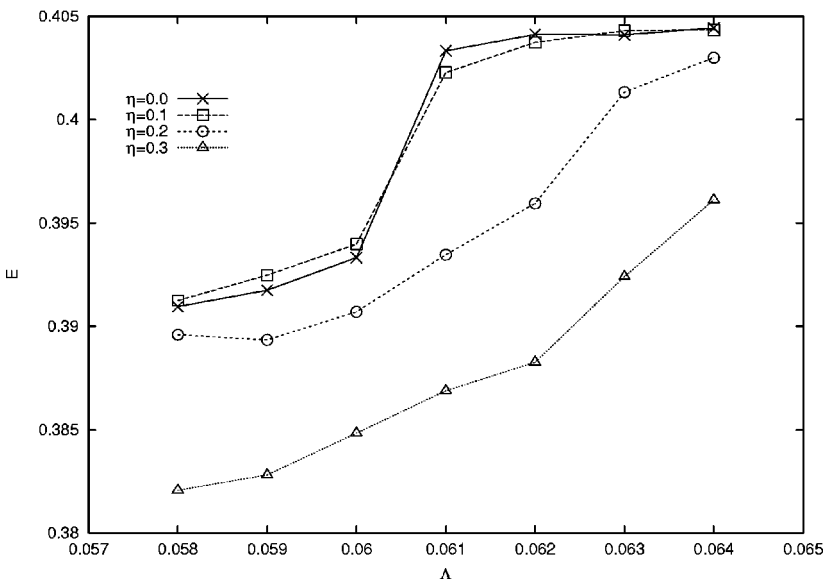

FIG. 2. YBCO: Energy as a function of Λ for $N=36$. A jump in the energy is seen up to $\eta =0.1$. For $\eta \geq 0.2$, the rise in the energy is soothed out.
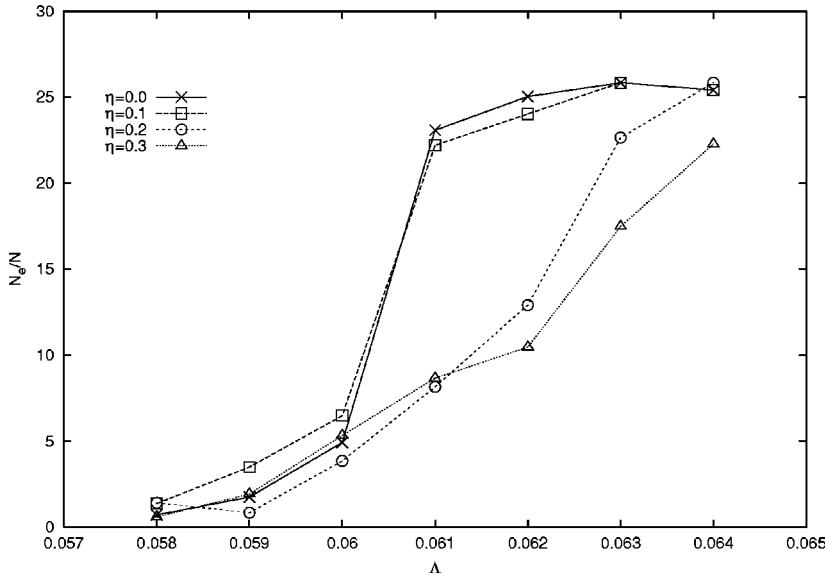
FIG. 3. YBCO: Fraction of entangled FL's as a function of Λ. For $\eta \lesssim 0.1$, a sharp jump in the FL entanglement is seen. For $\eta \gtrsim 0.2$, the rise of N_e/N with Λ becomes gradual as compared with the clean system.

For the pure system ($\eta = 0$), we see a sharp jump in the energy at exactly the point where the translational as well as hexatic structure factors sharply decline. This jump in energy is a clear signature of a first-order transition. From the energy jump we can compute the jump in entropy Δs. The jump in energy at the transition is around $\Delta E = 12.0k$ K per vortex per layer, which gives $\Delta s = \Delta E/T_m = 0.19k$, which is small compared to the experimental value of $\Delta s = 0.40k$ at $B \approx 125$ G. However, these values for Δs, T_m, and B are in qualitative agreement with the same system studied using a different model.[18]

Introduction of the columnar defects of a finite strength shows some interesting effects. We put columnar pins at random positions with a concentration fixed at 20% of the FL's. We study the BSCCO system for pins of low strength ($\eta = 0.2$) as well as for a higher strength ($\eta = 0.5$). Columnar disorder of strength up to $\eta = 0.2$ appear to have little effect on the system. This can be seen from the energy vs temperature graph in Figs. 5 and 6, where the curve for the pure

system and the one in the presence of low disorder strength ($\eta = 0.2$) fall on top of each other, except in the transition region where the jump in case of the system with columnar pins is more gradual. Also, from Figs. 7 and 8, we see that the $S(\mathbf{Q}_1)$ is not much affected in the presence of the columnar disorder of strength $\eta = 0.2$. The same is true for the hexatic order depicted in Fig. 9. This means that for the lower strengths of the disorder, the vortex-vortex interaction is dominant in the range of the temperature where we carried out simulations. As a result the first-order vortex-lattice melting transition line is almost not affected.

The nature of FL melting changes, however, when the strength of the disorder is increased to $\eta = 0.5$ as seen in Figs. 7 and 8. We see that at the lower temperatures the order parameter is suppressed. As we increase the temperature, the order parameter starts to rise and joins the melting curve of the pure system and then falls along it at even higher temperatures. Figure 9 indicates that the hexagonal structure factor also shows a similar behavior. This clearly shows that the
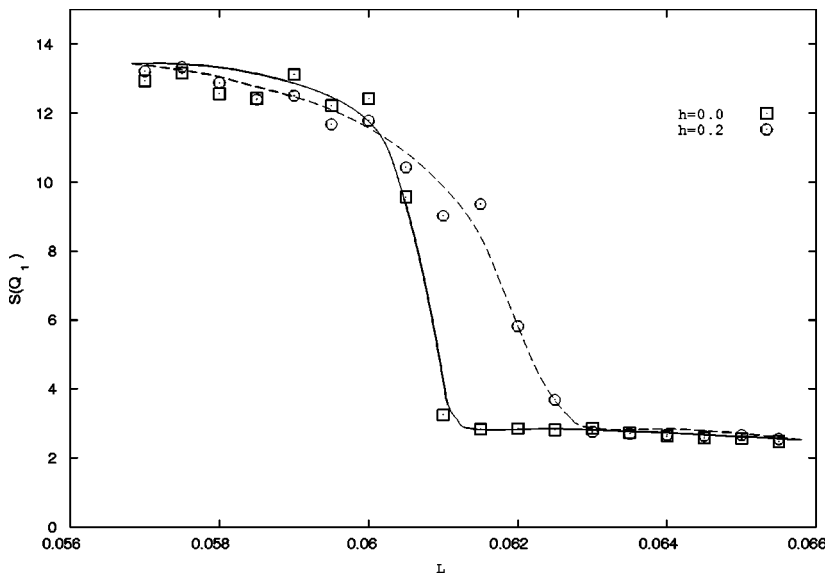

FIG. 4. YBCO: Structure factor at the first Bragg peak vs Λ for $N = 64$. Smooth lines are provided as a visual aid. Transition for $\eta = 0.0$ and $\eta = 0.2$ are seen almost at the same Λ's as with $N = 36$.
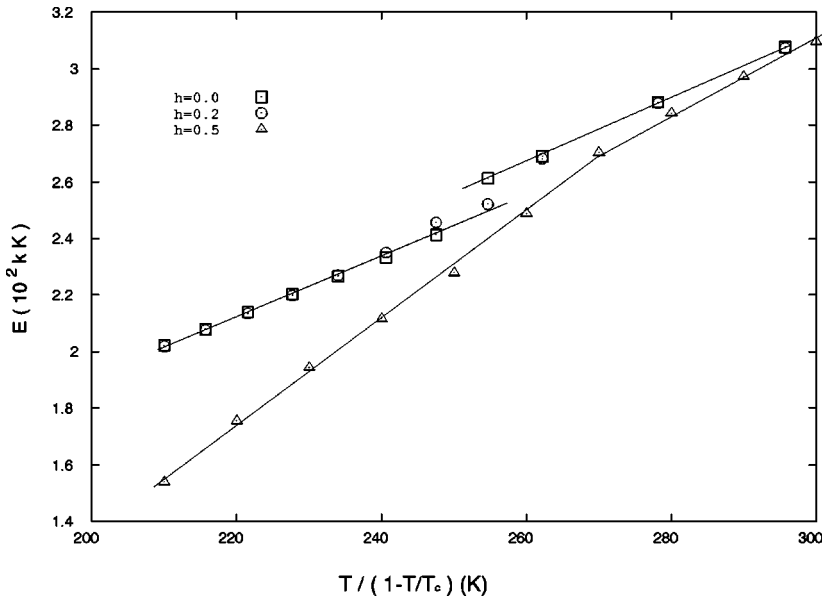
FIG. 5. BSCCO: Energy as a function of the reduced temperature for $\eta = 0, 0.2, 0.5$ at $B = 125$ G for $N = 36$. Lines were added to help visualize the energy jumps. A discontinuous change in energy is seen at $T_r = 250$, 260 K ($T \approx 66.2$, 66.9 K) for $\eta = 0$, 0.2, respectively. For $\eta = 0.5$, only a change in slope can be seen at $T_r \approx 268$ K ($T \approx 67.4$ K) instead of a discontinuous jump.

FL's start to disengage from the pinning centers as they wiggle more. At higher temperatures, columnar pins with the strength chosen here are not effective in pinning the vortex system. This becomes clear from the fact that the melting curve for the pure system and the one with columnar disorder join each other at a temperature below the FOT. Further interpretation and a possible explanation of this phenomenon will be discussed in more detail in the Conclusions section below. This convergence of the curves for the pure and disordered cases is also borne out in the E vs T graphs in Figs. 5 and 6. Initially at low temperatures, there is a big difference in energies of the systems with no disorder ($\eta = 0.0$) and high disorder ($\eta = 0.5$). However, as the temperature is increased, the two curves come closer and finally merge together in the liquid phase. The jump in energy in the presence of columnar defects can still be seen in the E vs T graph for a disorder strength of $\eta = 0.2$. This tends to suggest that the FOT in a BSCCO system is not affected by disorders

kept at as many as 20% of the total number of lines used in the simulations as long as we keep the strength of the disorder less or equal to $\eta = 0.2$. For $\eta = 0.5$, the rise of energy with temperature becomes much more gradual and we do not see any discontinuous jump in energy at any temperature. On the other hand, an abrupt change in slope of the energy vs temperature graph is observed, suggesting a discontinuity in the specific heat characterizing a second-order transition.

In Figs. 10 and 11, the snapshots of FL's, projected on a plane, at temperatures less than the transition temperature and at a temperature bigger than the transition temperature are shown. From Fig. 10, it is easily seen that at low temperatures most columnar defects have captured FL's. Also, the FL's make simple loops and have cleverly set themselves so as to make a hexagonal lattice and yet occupy as many defects as possible. The transverse fluctuations of the trapped FL's are greatly suppressed at low temperatures. At higher temperature beyond the transition point, we see that colum-
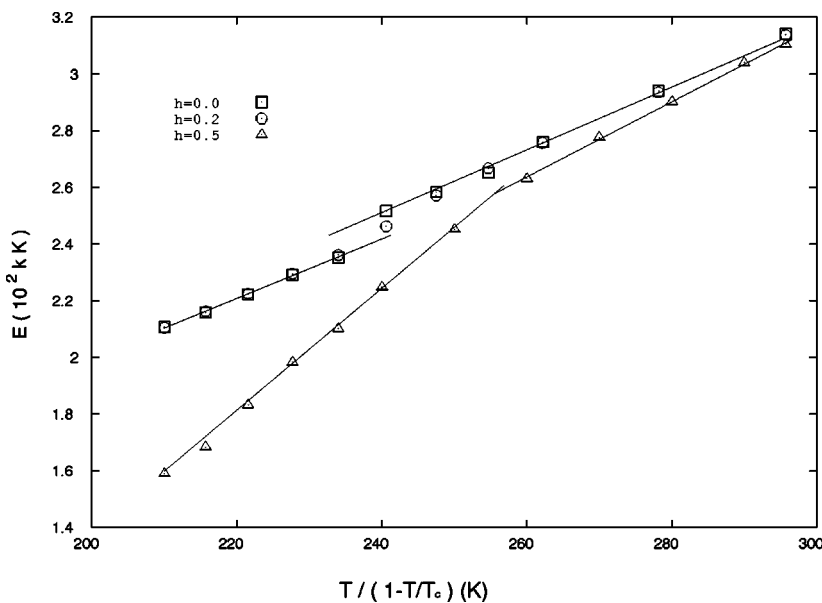

FIG. 6. BSCCO: Energy as a function of the reduced temperature for $\eta = 0$, 0.2, 0.5 at $B = 125$ G for $N = 64$. A jump in energy can be seen at $T_r \approx 238$, 242 K ($T \approx 65.3$, 65.6 K) for $\eta = 0, 0.2$, respectively. Again no discontinuity is observed for $\eta = 0.5$, but only a change in slope at $T_r \approx 255$ K ($T \approx 66.5$ K).
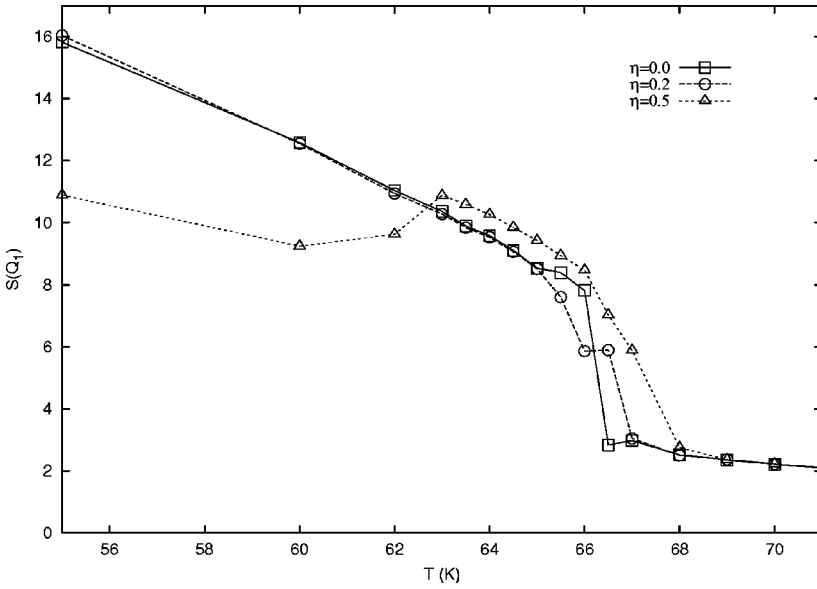
FIG. 7. BSCCO: Structure factor at the first Bragg peak vs temperature at $B = 125$ G for $N = 36$. No shift in transition point is seen for $\eta = 0.2$. In the presence of columnar pins with $\eta = 0.5$, the transition temperature increases from 66 K to 68 K. Also, we can see that $S(\mathbf{Q}_1)$ starts to rise close to 60 K.

nar defects are not occupied any more and a lot of FL's are entangled.

Inspection of snapshots like Fig. 10 gives support to the assertion of Sen *et al.* that the Bose glass consists of patches of ordered regions with only short-range positional and orientational order. This phase is different from the Bragg glass in systems with point pins which is characterized by quasi-long-range order.

Figure 12 shows the mean-squared displacements of the FL's in the z direction at different temperatures for a pure system. At lower temperatures $u^2(z)$ saturates for large z but in the liquid state it grows linearly.[17] A large gap in $u^2(z)$ for large values of z seen at the transition temperature signals the onset of the entanglement of the FL's.

In the presence of the columnar disorder of the strength $\eta = 0.5$, we see from Fig. 13 that $u^2(z)$ at temperatures less than the transition temperature is suppressed compared to the corresponding $u^2(z)$ in the pure system. This result is in

agreement with the findings in Ref. 25. Also the big gap in $u^2(z)$ occurring at the melting transition has moved towards a higher temperature signaling a shift in the position of the melting transition in the presence of columnar defects.

VI. CONCLUSIONS

For lower strengths of disorder ($\eta \leq 0.1$ for YBCO and $\eta \leq 0.2$ for BSCCO) no appreciable shift in the melting line was seen. For these strengths, a sharp drop in the translational and hexatic structure factors takes place at the transition. Also, the jump in energy at the transition is not affected much as compared with the case when there is no disorder present. This suggests that for smaller concentrations of the columnar defects the transition still remains first order. This result is in agreement with Ref. 36, where even with the introduction of the columnar disorder no shift in transition
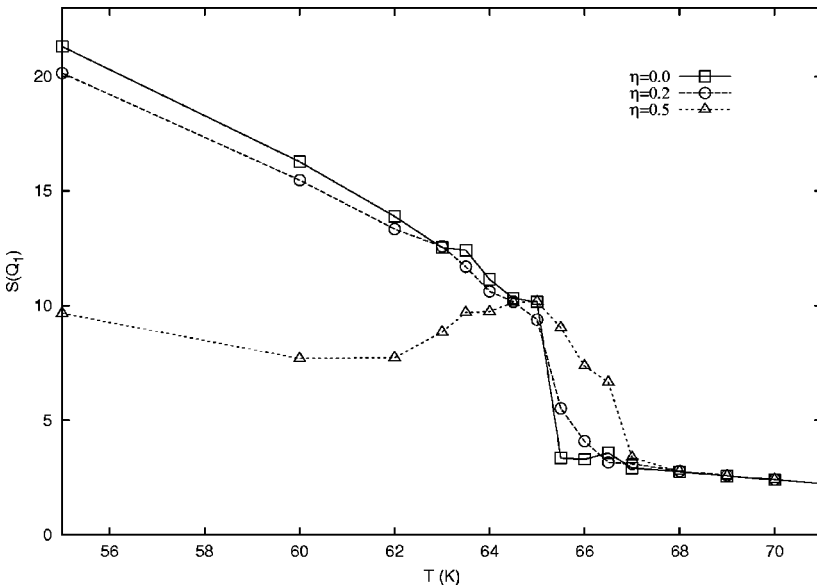

FIG. 8. BSCCO: Structure factor at the first Bragg peak vs temperature at $B = 125$ G for $N = 64$. For $\eta = 0.2$, no significant change in the structure factor is observed. In the presence of columnar pins with $\eta = 0.5$, transition temperature increasing from 65 K to 67 K. Also, we can see that $S(\mathbf{Q}_1)$ starts to rise close to 61 K.
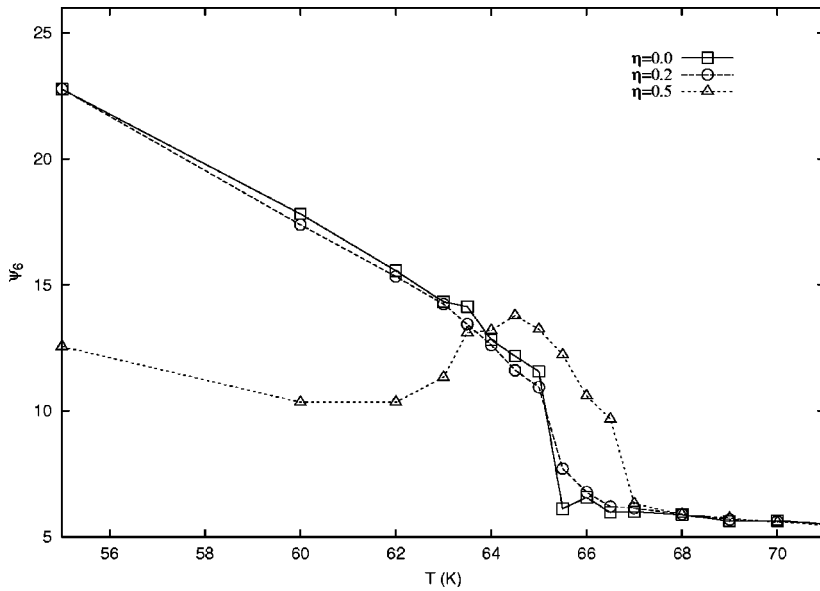
FIG. 9. BSCCO: Hexatic order vs temperature at $B = 125$ G for $N = 64$. When compared with the previous figure, it can be seen that ψ_6 almost follows $S(\mathbf{Q}_1)$.

temperatures is seen as long as the concentration of columnar disorder introduced is small.

It is found that for YBCO as well as BSCCO, the melting transition shifts towards higher values of temperature and magnetic field when random disorder is introduced provided its strength exceeds a threshold which is different for YBCO and BSCCO. The size of the shift, for a given concentration of defects, depends on the strength of the disorder. For YBCO, a considerable shift in the melting line towards higher temperatures and magnetic fields was seen for $\eta = 0.2$ and $\eta = 0.3$. This shift was bigger for $\eta = 0.3$ than for $\eta = 0.2$. Similarly, for BSCCO, a large shift in the melting line towards a higher temperature was found for $\eta = 0.5$. These results are in tune with numerous experimental findings[27,28,30,36] as well as theoretical prediction[25] where the irreversibility line is seen to shift towards higher temperature and magnetic fields in the presence of columnar defects. The qualitative reason for this effect is that due to the interaction with the columnar defects the transverse thermal fluctuations

of the FL's are reduced and thus the melting transition, as determined from the Lindemann criterion, takes place at at a higher temperature.

At $\eta = 0.5$, the jump in energy is not discernible any more. Instead, a change of slope corresponding to a specific-heat discontinuity is observed. This means that the transition is probably not of first order in the presence of columnar disorder of higher strengths, but it is rather a continuous (second-order) transition.

The most dramatic outcome of this study for BSCCO is that for some values of the applied field and defect strength both the translational and hexatic structure factors start to rise at a certain temperature as the transition is approached from the lower-temperature side. This is an unusual result, that to our knowledge, has not been seen in previous simulations. This fact can be explained as follows. At low temperatures, the free energy is dominated by energy effects rather than entropy considerations, and pinning effects are dominant. As a result most columnar defects capture a FL,
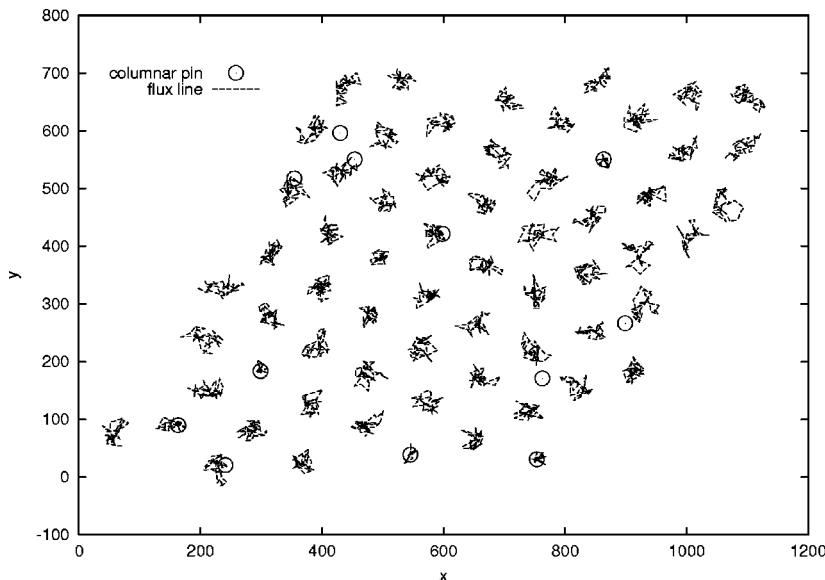

FIG. 10. BSCCO: A typical configuration in the solid phase (low temperature) for $N = 64$ FL's and $B_\phi/B = 0.2$. FL's have been projected onto one plane.
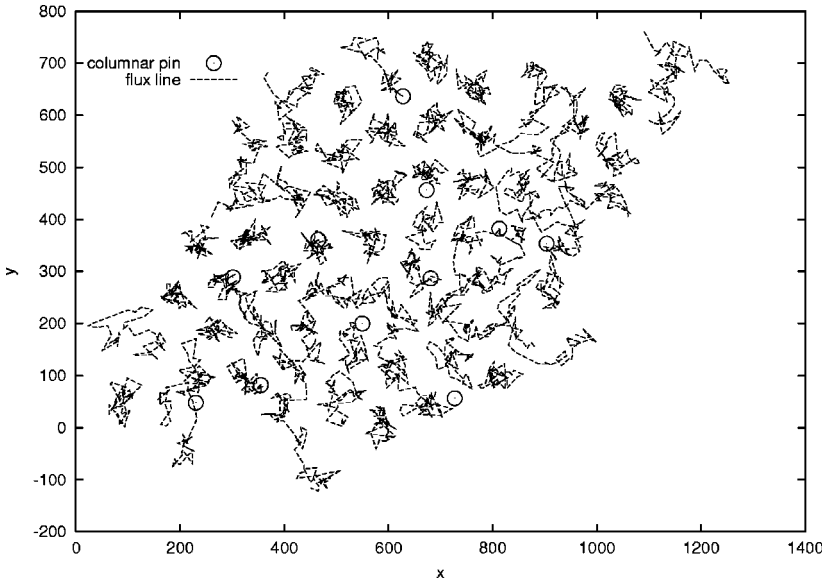
FIG. 11. BSCCO: A typical configuration of FL's in the liquid phase (high temperature) for $N=64$ and $B_\phi/B=0.2$. FL's have been projected onto a single plane. Columnar defects are not drawn to scale. Some FL's on the boundary do not seem to make loops. That is only because virtual images of FL's outside the cell are not shown.

while the rest of the FL's adjust themselves in positions such as to minimize the free energy. However, as the temperature is increased, FL's start to decouple from the defect sites, which allow the vortices pinned at interstitial positions to move themselves into a more ordered arrangement, thus increasing the structure factors compared to the situation at lower temperatures. As was mentioned before, due to its high anisotropy, FL's in BSCCO behave more like a collection of two-dimensional droplets rather than rigid rods. These two-dimensional droplet are comparatively more difficult to get pinned all at once by a columnar defect. On the other hand, FL's are much stiffer in YBCO and it is easier for a columnar defect to capture a FL all along its length. It can be shown [Eq. (9.49) in Ref. 2] that the depinning temperature for FL's, T_{dp}, is inversely proportional to the anisotropy parameter γ. Thus, we expect FL depinning to occur at comparatively smaller temperatures in BSCCO than in YBCO. Since the melting temperatures are not that different between these materials at the fields we consider, the depinning process for

BSCCO occurs further below the melting temperature than in YBCO. This allows the structure factor to increase above the depinning temperature before its ultimate decline at the melting transition. For YBCO, the depinning takes place close to the melting temperature, and it is difficult to detect any rise in the structure factors, especially for small systems, because it is masked by the decrease in order due to the stronger thermal fluctuations.

In principle, the rise of the order parameters in the presence of low amount of columnar defects as the melting transition temperature is approached could be observed experimentally, if the appropriate parameters are tuned correctly. In small-angle neutron scattering (SANS)[11,37] one can measure the integrated intensity over a Bragg peak of wave vector $\mathbf{Q}_1$ which is proportional to the translational structure factor $S(\mathbf{Q}_1)$ measured in the simulation. Another commonly used technique is muon spin rotation[37] which gives information about the width of the magnetic-field distribution in the sample. This is not directly proportional to the structure fac-
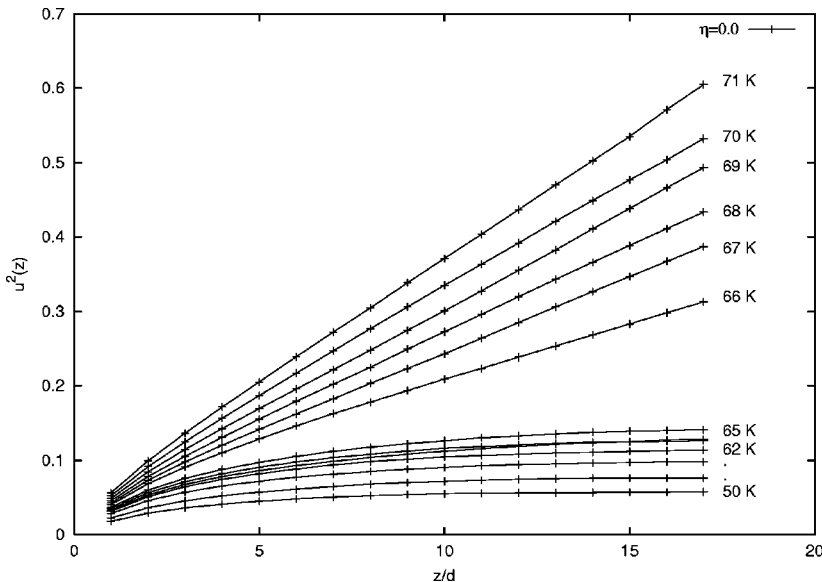

FIG. 12. BSCCO: Line wandering along the z direction at $B=125$ G for $N=64$. Here, d is the distance between adjacent planes. A large increase in line wandering occurs at $T\approx 65$ K.
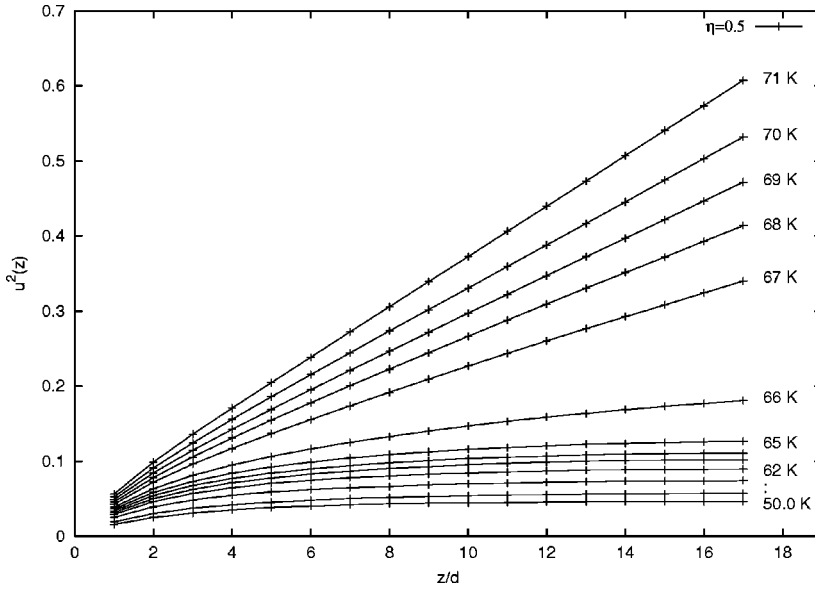
FIG. 13. BSCCO: Line wandering along the z direction at $B=125$ G for $N=64$ in the presence of disorder of strength $\eta=0.5$. The big jump in $u^2(z)$ has moved to $T=66$ K now.

tor at a given $\mathbf{Q}_1$, but is rather given by

$$\langle \Delta B^2 \rangle (T) = B^2 \sum_{\mathbf{Q} \neq 0} \frac{\exp(-\mathbf{Q}^2 \langle u^2 \rangle / 2)}{[1+\lambda^2(T)\mathbf{Q}^2]^2}, \qquad (6.1)$$

where $\langle u^2 \rangle$ is the mean-square deviation of vortices from their average position. It is possible to measure this quantity in the simulations but this was not done in the present work. This quantity might not show the unusual rise describe above since it is dominated by $\langle u^2 \rangle$ which is very likely monotonically increasing with temperature yielding a monotonically decreasing linewidth. Thus, in order to look for the effect observed in this paper, we suggest using the SANS technique to look at a BSCCO sample with columnar pins described by a matching field of about 25 G and an applied field of about 125 G. It is not clear to us what is the corresponding η parameter describing the pinning strength of the experimental defects. According to Blatter *et al.*[2] η lies in the range 0.1–1.

Note added. After this paper has been submitted we learned of two recent experimental studies of BSCCO by S. S. Banerjee *et al.*[55] and M. Menghini *et al.*[56] who study the melting transition for $B > B_\phi$. Our findings, especially our Fig. 10, are consistent with their ''crystallites in the pores'' picture of the ordered phase in the presence of columnar defects.

ACKNOWLEDGMENTS

APPENDIX A: ENERGY SUM OVER THE IMAGES

Consider a rhombically shaped region with side L and angle θ, unit vectors are $\mathbf{e}_1$, $\mathbf{e}_2$, with $\mathbf{e}_1 \cdot \mathbf{e}_2 = \cos \theta$. In practice, we took $\theta=60°$ but we leave the discussion here more general. The Green's function G_0 which describe the 2D Coulomb interaction between one vortex and another including all its images, as is implied by the periodic boundary conditions is given by the solution to London's equation (see, e.g., Ref. 1)

$$(1-\lambda^2 \nabla^2) G_0(\mathbf{R}, \lambda) = 2\pi\lambda^2 \delta(\mathbf{R}), \qquad (A1)$$

with the parameter λ setting the scale for the range of the interaction. The solution is given by

$$G_0(\mathbf{R}, \lambda) = \frac{2\pi\lambda^2}{L^2 \sin \theta} \sum_{\mathbf{Q}} \frac{\exp(i\mathbf{Q} \cdot \mathbf{R})}{1+\lambda^2 \mathbf{Q}^2}, \qquad (A2)$$

with

$$\mathbf{R} = R_1 \mathbf{e}_1 + R_2 \mathbf{e}_2, \quad \mathbf{Q} = n_1 \mathbf{b}_1 + n_2 \mathbf{b}_2, \qquad (A3)$$

where $\mathbf{Q}$ runs over all reciprocal-lattice vectors spanned by

$$\mathbf{b}_i = \frac{2\pi}{L \sin^2 \theta}(\mathbf{e}_i - \mathbf{e}_j \cos \theta), \qquad (A4)$$

for $(i,j) = (1,2),(2,1)$. Substituting in Eq. (A2), we obtain

$$G_0(\mathbf{R}, \lambda) = \frac{\sin \theta}{2\pi} \sum_{n_1 = -\infty}^{\infty} \sum_{n_2 = -\infty}^{\infty} \frac{\exp\left[i\frac{2\pi}{L}(n_1 R_1 + n_2 R_2)\right]}{L^2 \sin^2 \theta / (2\pi\lambda)^2 + n_1^2 - 2n_1 n_2 \cos \theta + n_2^2}. \qquad (A5)$$

We are now going to carry out the summation over n_1 analytically. This can be done by using the formula

$$\sum_{n=-\infty}^{\infty} f(n) = -\sum \left[\text{residues of } \pi f(z)(\cot \pi z - i) \right.$$
$$\left. \text{at poles of } f(z) \right]. \tag{A6}$$

We have subtracted the constant i from $\cot \pi z$ to ensure that $|zf(z)(\cot \pi z - i)| \rightarrow 0$ on the contour of integration when z has a large negative imaginary component. The contour of integration is a square with sides parallel to the real and imaginary axes with the origin in the middle, in the limit that its size goes to infinity. In our case

$$f(z) = \frac{e^{ixz}}{(z-\beta-i\gamma)(z-\beta+i\gamma)}, \tag{A7}$$

with appropriate values of β, γ, and x. This function has two simple poles, and the residues can be easily evaluated. The final answer becomes (relabeling n_2 as n)

$$G_0(\mathbf{R},\lambda) = \frac{\sin \theta}{2} \sum_{n=-\infty}^{+\infty} \frac{\cos(t_2 n - 2\pi\beta_n)\sinh(\gamma_n t_1) + \cos(t_2 n)\sinh[\gamma_n(2\pi - t_1)]}{\gamma_n[\cosh(2\pi\gamma_n) - \cos(2\pi\beta_n)]}, \tag{A8}$$

where

$$t_1 = \frac{2\pi R_1}{L}, \quad t_2 = \frac{2\pi}{L}(R_1 \cos \theta + R_2), \quad \beta_n = n \cos \theta,$$

$$\gamma_n = \sin \theta \sqrt{n^2 + L^2/(2\pi\lambda)^2}. \tag{A9}$$

This expression is simpler than the one used by Nordborg and Blatter since it does not have different expressions for even and odd n. It also converges faster in certain regions.

APPENDIX B: PERMUTATION SAMPLING

Essentially the same method is used for permutation sampling as was used in Ref. 19. The only difference is that we use permutation space of only the neighboring lines. This is so because even if we were able to get a permutation step,

involving a large number of lines, accepted at the first stage of the algorithm, it would be very likely to get rejected at the following stages. So we work with only three to five lines. Sufficiently long segments (typically five planes) of a number of lines were cut. Care should be taken to make sure that chosen FL's are the nearest neighbors in the plane where the reconnection of FL's is going to take place. These points can be implemented easily with the concept of linked lists and pointers.[54] Also, care is to be taken that even though a FL may be far away from some other FL in the rhombically shaped unit cell, it can still permute with it through one of the images of the latter. These few simple points are very important to implement the whole procedure correctly. Just for a check, we tried with the sampling procedure given in Ref. 46. This gave results in good agreement with the sampling procedure given above.

[1] M. Tinkham, *Introduction to Superconductivity*, (McGraw-Hill, New York, 1975).

[2] G. Blatter, M.V. Feigel'man, V.B. Geshkenbein, A.I. Larkin, and V.M. Vinokur, Rev. Mod. Phys. **66**, 1125 (1994), and references therein.

[3] E.H. Brandt, Rep. Prog. Phys. **58**, 1465 (1995).

[4] A.A. Abrikosov, Zh. Éksp. Teor. Fiz. **32**, 1442 (1957) [Sov. Phys. JETP **5**, 1174 (1957)].

[5] E. Brezin, D.R. Nelson, and A. Thiaville, Phys. Rev. B **31**, 7124 (1985).

[6] F. Lindemann, Phys. Z. **11**, 69 (1910).

[7] D.R. Nelson and H.S. Seung, Phys. Rev. B **39**, 9153 (1989).

[8] A. Houghton, R.A. Pelcovits, and A. Sudbo, Phys. Rev. B **40**, 6763 (1989); **42**, 906 (1990).

[9] H. Safar, P.L. Gammel, D.A. Huse, D.J. Bishop, J.P. Rice, and D.M. Ginsberg, Phys. Rev. Lett. **69**, 824 (1992).

[10] W.K. Kwok, S. Fleshler, U. Welp, V.M. Vinokur, J. Downey, G.W. Crabtree, and M.M. Miller, Phys. Rev. Lett. **69**, 3370 (1992).

[11] R. Cubitt, E.M. Forgan, G. Yang, S.L. Lee, D.M. Paul, H.M. Mook, M. Yethiraj, P.H. Kes, T.W. Li, A.A. Menovsky, Z. Tarnavski, and K. Mortensen, Nature (London) **365**, 407 (1993).

[12] E. Zeldov, D. Majer, M. Konczykowski, V.B. Geshkenbein, V.M. Vinokur, and H. Shtrikman, Nature (London) **375**, 373 (1995).

[13] A. Schilling, R.A. Fisher, N.E. Phillips, U. Welp, D. Dasgupta, W.K. Kwok, and G.W. Crabtree, Nature (London) **382**, 791 (1996).

[14] S. Sengupta, C. Dasgupta, H.R. Krishnamurthy, G.I. Menon, and T.V. Ramakrishnan, Phys. Rev. Lett. **67**, 3444 (1991).

[15] W.R. Magro and D.M. Ceperley, Phys. Rev. B **48**, 411 (1993).

[16] S. Ryu, S. Doniach, G. Deutscher, and A. Kapitulnik, Phys. Rev. Lett. **68**, 710 (1992); S. Ryu, Ph.D. thesis, Stanford University, 1995.

[17] A.E. Koshelev, Phys. Rev. B **56**, 11 201 (1997).

[18] X. Hu, S. Miyashita, and M. Tachiki, Phys. Rev. B **58**, 3438 (1998).

[19] H. Nordborg and G. Blatter, Phys. Rev. B **58**, 14 556 (1998).

[20] S.-K. Chin, A.K. Nguyen, and A. Sudbo, Phys. Rev. B **59**, 14 017 (1999).

[21] T. Giamarchi and P. Le Doussal, Phys. Rev. B **52**, 1242 (1995).

[22] T. Nattermann and S. Scheidl, Adv. Phys. **49**, 607 (2000).

[23] G.I. Menon and C. Dasgupta, Phys. Rev. Lett. **73**, 1023 (1994).

[24] D. Ertas and D.R. Nelson, Physica C **272**, 79 (1996).

[25] Y.Y. Goldschmidt, Phys. Rev. B **56**, 2800 (1997).

[26] D.R. Nelson and V.M. Vinokur, Phys. Rev. Lett. **68**, 2398 (1992); Phys. Rev. B **48**, 13 060 (1993).

[27] M. Konczykowski, F. Rullier-Albenque, E.R. Yacoby, A. Shaulov, Y. Yeshurun, and P. Lejay, Phys. Rev. B **44**, 7167 (1991).

[28] L. Civale, A.D. Marwick, T.K. Worthington, M.A. Kirk, J.R. Thompson, L. Krusin-Elbaum, Y. Sun, J.R. Clem, and F. Holtzberg, Phys. Rev. Lett. **67**, 648 (1991).

[29] A.V. Samoilov, M.V. Feigel'man, M. Konczykowski, and F. Holtzberg, Phys. Rev. Lett. **76**, 2798 (1996).

[30] L.M. Paulius, J.A. Fendrich, W.K. Kwok, A.E. Koshelev, V.M. Vinokur, G.W. Crabtree, and B.G. Glagola, Phys. Rev. B **56**, 913 (1997).

[31] R.J. Olsson, W.-K. Kwok, L.M. Paulius, A.M. Petrean, D.J. Hofman, and G.W. Crabtree, Phys. Rev. B **65**, 104520 (2002).

[32] W. Gerhauser, G. Ries, H.W. Neumuller, W. Schmidt, O. Eibl, G. Saemann-Ischenko, and S. Klaumunzer, Phys. Rev. Lett. **68**, 879 (1992).

[33] L. Klein, E.R. Yacoby, Y. Yeshurun, M. Konczykowski, and K. Kishio, Phys. Rev. B **48**, 3523 (1993).

[34] M. Konczykowski, N. Chikumoto, V.M. Vinokur, and M.V. Feigelman, Phys. Rev. B **51**, 3957 (1995).

[35] W.S. Seow, R.A. Doyle, A.M. Campbell, G. Balakrishnan, D.McK. Paul, K. Kadowaki, and G. Wirth, Phys. Rev. B **53**, 14611 (1996).

[36] B. Khaykovich, M. Konczykowski, K. Teitelbaum, E. Zeldov, H. Shtrikman, and M. Rappaport, Phys. Rev. B **57**, R14 088 (1998).

[37] S.L. Lee, C.M. Aegerter, S.H. Lloyd, E.M. Forgan, C. Ager, M.B. Hunt, H. Keller, I.M. Savic, R. Cubitt, G. Wirth, K. Kadowaki, and N. Koshizuka, Phys. Rev. Lett. **81**, 5209 (1998).

[38] C.J. van der Beek, M. Konczykowski, A.V. Samoilov, N. Chiku-moto, S. Bouffard, and M.V. Feigel'man, Phys. Rev. Lett. **86**, 5136 (2001).

[39] C.J. van der Beek, M. Konczykowski, R.J. Drost, P.H. Kes, N. Chikumoto, and S. Bouffard, Phys. Rev. B **61**, 4259 (2000).

[40] L. Radzihovsky, Phys. Rev. Lett. **74**, 4923 (1995).

[41] C. Wengel and U.C. Täuber, Phys. Rev. B **58**, 6565 (1998).

[42] P. Sen, N. Trivedi, and D.M. Ceperley, Phys. Rev. Lett. **86**, 4092 (2001).

[43] A. Nandgaonkar, D.G. Kanhere, and N. Trivedi, Phys. Rev. B **66**, 104527 (2002).

[44] D.R. Nelson, Phys. Rev. Lett. **60**, 1973 (1988).

[45] A.D. Klemm and R.G. Storer, Aust. J. Phys. **26**, 43 (1973).

[46] D.M. Ceperley, Rev. Mod. Phys. **67**, 279 (1995).

[47] W.E. Lawrence and S. Doniach, in *Proceedings of LT 12, Kyoto, 1970*, edited by E. Kanda (Keigaku, Tokyo, 1971), p. 361; S. Doniach, in *High Temperature Superconductivity*, Proceedings of the Los Alamos Symposium, 1989, edited by K.S. Bedell *et al.* (Addison-Wesley, Redwood City, 1989), p. 406.

[48] M.V. Feigel'man, V.B. Geshkenbein, and A.I. Larkin, Physica C **167**, 177 (1990).

[49] J.R. Clem, Phys. Rev. B **43**, 7837 (1991).

[50] S.N. Artemenko and A.N. Kruglov, Phys. Lett. A **143**, 485 (1990).

[51] G. Blatter, V. Geshkenbein, A. Larkin, and H. Nordborg, Phys. Rev. B **54**, 72 (1996).

[52] C.J. Olson, G.T. Zimányi, A.B. Kolton, and N. Gronbech-Jensen, Phys. Rev. Lett. **85**, 5416 (2000).

[53] S. Tyagi and Y.Y. Goldschmidt (unpublished).

[54] M.P. Allen and D.J. Tildesley, *Computer Simulation of Liquids* (Clarendon Press, Oxford, 1987).

[55] S.S. Banerjee, A. Soibel, Y. Myasoedov, M. Rappaport, E. Zeldov, M. Menghini, Y. Fasano, F. de la Cruz, C.J. van der Beek, M. Konczykowsky, and T. Tamegai, Phys. Rev. Lett. **90**, 087004 (2003).

[56] M. Menghini, Y. Fasano, F. de la Cruz, S.S. Banerjee, Y. Myasoedov, E. Zeldov, C.J. van der Beek, M. Konczykowsky, and T. Tamegai, cond-mat/0210623 (unpublished).